Research Article

Hacettepe University Journal of the Faculty of Pharmacy
Volume 44 / Number 3 / September 2024 / pp. 198-219

GC-MS Analysis, Antioxidant, Antidiabetic Activity, and ADMET Study of *Diospyros mespiliformis* Hochst. Ex A. DC. Ebenaceae Stembark

Mubarak Muhammad DAHIRU[1]
ORCID: 0000-0002-1252-3699
Neksumi MUSA[2]
ORCID: 0000-0003-1389-021X

[1]Department of Pharmaceutical Technology, School of Science and Technology,
Adamawa State Polytechnic, Yola, Jimeta, Adamawa State, Nigeria.

[2]Department of Science Laboratory Technology, School of Science and Technology,
Adamawa State Polytechnic, Yola, Jimeta, Adamawa State, Nigeria.

Corresponding author:
Mubarak Muhammad DAHIRU
Department of Pharmaceutical Technology, School of Science and Technology, Adamawa State Polytechnic, Yola, Jimeta, Adamawa State, Nigeria.

E-mail: mubaraq93@adamawastatepoly.edu.ng
Tel: +2348036508768

Received date : 07.09.2023
Accepted date : 08.07.2024

DOI: 10.52794/hujpharm.1356537

ABSTRACT

The present study carried out GC-MS analysis, antioxidant, antidiabetic, and ADMET study of the crude ethanol extract (CRE), ethyl acetate (EAF), and aqueous (AQF) fractions of *Diospyros mespiliformis* (DM). Grandiflorenic and cis, cis-linoleic acids were the most abundant of the 59 and 40 compounds identified in the EAF and AQF, respectively. The EAF and CRE exhibited significantly ($p < 0.05$) higher total antioxidant capacity than the AQF. Furthermore, the EAF exhibited a significantly ($p < 0.05$) higher percentage inhibition via the ferric thiocyanate assay than the CRE and AQF. All the extracts showed significantly ($p < 0.05$) lower malondialdehyde concentrations than AA in the thiobarbituric acid assay. Diazoprogesterone identified in the EAF exhibited the lowest binding affinity and inhibition constant, interacting with myeloperoxidase (MPO), xanthine (XO), and 11-β-hydroxysteroid dehydrogenase (HSD1), and sirtuin 6 (SIRT6). The molecular dynamics simulations showed residue fluctuations of the diazoprogesterone docked complexes with the highest observed at Ser42, Cys1325, Ser281, and Leu78 for MPO, XO, HSD1, and SIRT6, respectively. Moreover, diazoprogesterone was predicted to possess good ADMET properties. Conclusively, DM possesses significant antioxidant and antidiabetic potential, containing compounds that might be a source of novel therapeutics against oxidative stress and diabetes.

Keywords: Diabetes, Diazoprogesterone, Molecular docking, Molecular dynamics, Oxidative stress

1. Introduction

The persistent hyperglycemia associated with diabetes has been regarded as the culprit leading to diabetic complications and the manifestation of micro- and macro-vascular complications associated with diabetes, often initiated by oxidative stress [1-4]. A redox imbalance is created in diabetic subjects *via* free radical generation coupled with the depletion of the inherent antioxidant system of the body [5-9]. These free radicals damage cellular components, including membrane lipids and proteins through lipid peroxidation and deoxyribonucleic acids (DNA) [10]. In diabetes, persistent hyperglycemia affects multiple pathways, leading to the generation of free radicals. This includes the superoxide-dependent pathway for the peroxidation of LDL-C and glucose oxidation which generates superoxide [2-4, 11]. Additionally, the glycation of the antioxidant enzymes by hyperglycemia renders them inactive, further exacerbating oxidative stress in diabetes [11]. Therefore, a need for exogenous antioxidants to alleviate diabetic micro- and macro-vascular complications.

Different proteins were previously reported as targets of diabetic and oxidative stress therapy [12-14]. These proteins are associated with the pathology of diabetes, including hydroxysteroid 11-beta dehydrogenase 1 (HSD1) and sirtuin 6 (SIRT6) while others promote the generation of free radicals, leading to increased oxidative stress, including myeloperoxidase (MPO) and xanthine oxidase (XO). In most of the cases, these targets are often associated with pathways or transcription factors that promote hyperglycemia. Thus, inhibition of these pathways is associated with beneficial effects in diabetic subjects. HSD1 and SIRT6 are linked to glucose metabolism, especially glucose intolerance, lipid profile, and insulin resistance. HSD1 is linked to insulin resistance, wound healing, nephropathy, and macrovascular complications [15, 16]. SIRT6 is associated with diabetic complications, including diabetic cardiomyopathy, insulin resistance and inflammatory responses, microvascular function, and cardiovascular complications [17, 18]. However, some studies suggest potential beneficial effects of SIRT6 inhibition, leading to improved glycolysis and glucose uptake in muscles *via* GLUT 1 and 2, in addition to suppressing insulin resistance [19, 20]. MPO and XO activities are linked to free radical generation, exacerbating diabetic pathology. MPO mediates oxidative stress *via* reactive oxygen and nitrogen species generation and hypohalous acids synthesis. Inhibition of MPO reduces oxidative stress and inflammation linked to diabetes [21, 22]. XO inhibition prevents XO-induced oxidative stress and inflammation in diabetes by decreasing uric acid levels [23].

The recommended remedy for diabetes is exercise and good dieting though the use of drugs is also in practice [24]. However, the multifactorial nature of diabetes coupled with the undesirable side effects of the drugs complicates the management of the ailment. This often leads to multiple doses and combined therapy of different drugs to achieve glycemic control and suppress the chronic complications of diabetes [24]. Additionally, the side effects and cost of anti-diabetic drugs make them an undesirable remedy for many individuals. Remedies from plant sources are regarded as alternatives mainly due to their availability, affordability, and efficacy [25]. Moreover, in most cases, no associated side effects exist while bringing about relief to symptoms by alleviating oxidative stress due to their antioxidant properties [13, 26-29]. The pharmacological effects of plant-based drugs are often attributed to their phytochemical components made up of different compounds with individual and synergistic effects, targeting different ailments [30]. The multifactorial nature of diabetes makes it an ideal target for these compounds, targeting different aspects of the disease and attenuating its symptoms.

Medicinal plants have been previously reported to exert different pharmacological properties, including antioxidant and antidiabetic activities [25, 27, 28, 31, 32]. *Diospyros mespiliformis* (DM) is a tree indigenous to Africa, belonging to the Ebenacea family and growing up to 25 m with attributed medicinal properties [33]. This plant has been previously linked to several pharmacological activities, including antioxidant [13, 34] and antidiabetic [13, 35] properties, attributed to their phytochemical components. Thus, further studies to identify the phytochemicals attributed to the antioxidant and antioxidant activities can be warranted. In our study, we carried out GC-MS analysis and determined the antioxidant (*in vitro* and *in silico*), and antidiabetic (*in silico*) activity of the CRE, EAF, and AQF of DM Hochst. Ex A. DC. Ebenaceae stembark to identify the compounds that might be responsible for the antioxidant and antidiabetic activity of the plant.

ISSN: 2458 - 8806

2. Materials and Methods

2.1. Plant

The sample of DM stem bark was obtained from the Mayo-belwa Area of Adamawa State, Nigeria. Plant authentication was done by Enoch Buba Badgal of the Forest Technology Department, Adamawa State Polytechnic, Yola where a voucher specimen (No. ASP/FT/091) was deposited. The sample was cleaned, air-dried under shade, and powdered with a blender.

2.2. Extraction and fractionation

Exactly 1 kg of the sample was macerated for a week in 70% ethanol (v/v) and filtered. This was followed by drying under reduced pressure at 40 Å with a rotary evaporator (Buchi Rotavapor R-200), yielding 95 g of the CRE. Exactly 50 g of the CRE was suspended to complete dissolution in 200 ml of distilled water and continuously partitioned in a separating funnel by the addition of ethyl acetate until the formation of a clear ethyl acetate layer to yield the EAF. The remaining aqueous layer was regarded as the AQF. The EAF and AQF were subjected to the same drying condition as the CRE to yield 10.60 and 36.80 g of the EAF and AQF, respectively.

2.3. Qualitative phytochemical test

The phytochemical components of DM were identified by the methods previously described for alkaloids, saponins, steroids, glycosides, terpenoids, and flavonoids [36, 37].

2.3.1. Alkaloids

To 2 ml of the extract, 2 ml of 10% HCl was added, followed by the addition of 2 ml of Meyer's reagent. The formation of an orange precipitate indicated a positive result.

2.3.2. Saponins

To 2 ml of the extract, 2 ml of distilled water was added. The mixture was agitated in a test tube for 5 min. The appearance of a layer of foam indicated a positive result.

2.3.3. Tannins

To 2 ml of the extract, 5 drops of 0.1% ferric chloride were added. The formation of a brownish-green or blue-black coloration indicated a positive result.

2.3.4. Steroids

To 2 ml of the extract, 10 ml of chloroform was added and then 10 ml of concentrated sulphuric acid was added by the side of the test tube. The formation of a reddish upper layer and yellow sulphuric acid layer with green fluorescence indicated a positive result.

2.3.5. Glycosides

Exactly 2 ml of acetic acid was added to 2 ml of the extract. The mixture was cooled in a cold-water bath, and then 2 ml of concentrated H_2SO_4 was added. Color development from blue to bluish-green indicated the presence of glycosides.

2.3.6. Terpenoids

To 2 ml of the extract, 2 ml of chloroform and 1 ml of concentrated sulphuric acid were carefully added to form a layer. A clear upper and lower layer with reddish-brown interphase indicated a positive result.

2.3.7. Flavonoids

To 2 ml of the extract, 10% sodium hydroxide was added. A yellow color was formed which turned colorless upon the addition of 2 ml of dilute hydrochloric acid, indicating a positive result.

2.4. Gas chromatography-mass spectroscopy (GC-MS)

The compounds present in EAF and AQF were identified using GC-MS as we described previously [38]. A combined GCMS instrument (Agilent 19091-433HP, USA) fitted with a silica column was used. The column flow velocity of the carrier gas (Helium) was set to 1.6 ml/min while the temperature and pressure were set to 250 °C and 8.6 psi, respectively. Exactly 1 µl was injected *via* split mode at 250 °C. The temperature was subjected to gradual increments at 20 °C/min to 180 °C after the initial start at 100 °C. Furthermore, the temperature was raised to 280 °C at 10 °C/min while the elusion time was set at 16 min. Identification of compounds was carried out *via* comparison with known spectrums from the National Institute of Standards and Technology database.

2.5. Antioxidant activity

2.5.1. Total reducing power (TRP)

The method previously described was followed to determine the TRP [39]. Exactly, 0.25 ml of the

sample (1 mg/ml) was mixed with 0.625 ml of 1% (w/v) potassium ferrocyanide and 0.625 ml of 0.2 M phosphate buffer (pH 6.6), followed by 20 min of incubation at 50 °C. Furthermore, 0.625 ml of 10% (w/v) trichloroacetic acid (TCA) was added and centrifuged at 3000 rpm for 10 min. Exactly, 1.8 ml of the upper layer was collected, followed by the addition of 1.8 and 0.36 ml of distilled water and 0.1% $FeCl_3$, respectively. The absorbance was read at 700 nm against a solution of the reagents without the sample (blank). The ascorbic acid (AA) calibration curve was obtained from different concentrations of AA (20-100 µg/ml) subjected to the same treatment as the sample. The TRP was expressed as ascorbic acid equivalent (mg AAE/g extract) of triplicate determinations using the AA standard calibration curve.

2.5.2. Total antioxidant capacity (TAC)

The phosphor-molybdenum protocol previously described [40] was followed to determine the TAC which was expressed as mg AAE/g extract of triplicate determinations, using the AA standard calibration curve. Exactly 0.5 ml of the sample (1 mg/ml) was added to 2 ml of phosphor-molybdate reagent (0.6 M H_2SO_4, 0.028 M sodium phosphate, and 1% ammonium molybdate), followed by capping and 10 min incubation at 95 °C. The absorbance was read at 695 nm against a blank of the solution of the reagents without a sample. The ascorbic acid calibration curve was obtained from different concentrations of AA (20-100 µg/ml) subjected to the same treatment as the sample.

2.5.3. Ferric thiocyanate method (FTC)

The inhibitory effect of the samples against lipid peroxidation (initial stage) was determined as described previously [41] and in triplicate determinations. Exactly, 4.1 and 4 ml of 2.52% (v/v) linolenic acid and 1 mg/ml of sample, respectively were dissolved in absolute ethanol. The solution was mixed with 0.05 M phosphate buffer (pH 7) and 3.9 ml of distilled water, followed by 10 min of dark-oven incubation at 40 °C. Furthermore, 0.1 ml of the solution was mixed with 9.7 ml of 75% (v/v) ethanol, 0.1 ml of 30% (w/v) ammonium thiocyanate, and 0.1 ml 0.02 M ferrous chloride in 3.5% (v/v) HCl. The absorbance was initially read 532 nm after adding ferrous chloride and continuously read every 24 h until the absorbance of the control reached maximum. Additionally, a solution of the reagents without the sample was used as blank while AA as standard. Equation 1 was used to determine the percentage inhibition.

$$\% \text{ Inhibition} = 100 - \left(\frac{\text{At}}{\text{Ac}} \times 100\right) \qquad \text{Equation 1}$$

Where At = Absorbance of the sample while Ac = Absorbance of control.

2.5.4. Thiobarbituric acid method (TBA)

The inhibitory effects of the samples on the late stage of lipid peroxidation were determined as described previously [41] and in triplicate determinations. Briefly, 1 ml of the sample and AA prepared from the FTC method were separately mixed with 2 ml of 20% (w/v) TCA and 2 ml of 0.5% (w/v) thiobarbituric acid solution, capped, and incubated for 10 min at 90 °C in a water bath and cooled. The mixture was centrifuged at 3000 rpm for 20 min and the absorbance of the supernatant was read at 532 nm on the last day of the FTC method. Additionally, a mixture of the reagents without the sample was used as blank while AA as standard. Equation 2 was used to evaluate the malonaldehyde (MDA) concentration using the extinction coefficient 156 mM-1 cm-1 as previously described [42].

$$\text{MDA concentration } \left(\frac{\text{nmol}}{\text{ml}}\right) = \left(\frac{\text{OD}}{\text{EC}} \times \text{Sample volume}\right) \qquad \text{Equation 2}$$

Where OD = Absorbance of the sample while EC = Extinction coefficient

2.5.5. Hydrogen peroxide (H2O2) scavenging assay

The titration procedure described previously was followed to determine the H_2O_2 scavenging potential of the samples [43]. All procedures were in triplicate. Two ml of 0.001 M hydrogen peroxide was mixed with the samples and 2 drops of 3% (w/v) ammonium molybdate, 10 ml of 0.2 M HCl, and 7 ml of 0.0018 M potassium iodide were added. This was followed by the addition of 2 drops of 1% (w/v) starch indicator. The mixture was titrated to the disappearance of the blue color with 0.0005 M sodium thiocyanate. A solution titrated without the extract was used as blank while AA as standard. All procedures were in triplicate. The peroxide scavenging activity was determined according to Equation 3.

ISSN: 2458 - 8806

$$\text{Hydrogen peroxide scavenging (\%)} = \frac{Vb-Vs}{Vb}\ x\ 100$$

Equation 3

Where Vb and Vs were the volume of sodium thiocyanate used to titrate blank and sample solutions, respectively.

2.6. In silico Study

2.6.1. Molecular Docking (MD) and Molecular Dynamics Simulation (MDS)

The identified compounds were initially screened by applying Lipinski's rule and Veber filter using the DruLiTo software to identify compounds with druglike properties. The structures of the compounds were downloaded from the PubChem website (https://pubchem.ncbi.nlm.nih.gov) in 3D SDF format while the targets (proteins) were downloaded from the RSCB protein data bank (https://www.rcsb.org). Heteroatoms, water molecules, and identical chains were removed from the targets using AutoDockTools software (version 1.5.7) [44] while the compounds were energy-minimized using the PyRx software (version 0.8) to prepare for docking. The PrankWeb: Ligand Binding Site Prediction online server (https://prankweb.cz) [45] was used to predict the binding pockets (grid box coordinates). The 2D and 3D interactions of the docked complexes were depicted using the LigPlot^{+} (version 2.2.8.) [46] and PyMol (Version 2.0 Schrödinger, LLC) software, respectively. The salt bridge was identified using the Protein-Ligand Interaction Profiler online server [47]. Table 1 shows the list of the top docked compounds with their PubChem ID.

The PyRx software (version 0.8) was used for the molecular docking with the exhaustiveness set to 16 while the grid box was as predicted. The top two compounds exhibiting the lowest binding energy (BA) were selected. Furthermore, Equation 4 was used to evaluate the inhibition constant (Ki) [48]. Moreover, only the top docked compounds are presented and subjected to the MDS. Table 2 displays the targets, including their RSCB ID and grid box coordinates. The Webnm server (http://apps.cbu.uib.no/webnma3) [49] and CABs-flex v2.0 (http://biocomp.chem.uw.edu.pl/CABSflex2/index) software [50] were employed for the MDS of the docked complexes to determine the cluster displacement and root-mean-square fluctuation (RMSF) of the residues, respectively.

$$Ki = \exp\left(\frac{\Delta G}{RT}\right)$$

Equation 4

where T=298.15 K (temperature), R=1.985 x 10^{-3} $kcal^{-1}$ mol^{-1} k^{-1} (the universal gas constant), and ΔG = binding affinity

2.6.2. ADMET Prediction

The pkCSM – pharmacokinetics online server (https://biosig.lab.uq.edu.au/pkcsm) was used to predict the absorption, distribution, metabolism, excretion, and toxicity (ADMET) of the compound with the lowest BA [51].

2.7. Statistics

The data obtained was statistically evaluated with Statistical Package for Social Sciences (SPSS) software version 22 and expressed as mean ± standard mean error. One-way analysis of variance was employed to evaluate the difference among the groups and subsequently evaluated by Turkey's multiple comparison tests at $p < 0.05$ significant level.

3. Results and Discussion

3.1. Phytochemical test

Table 3 presents the phytoconstituents present in DM. Saponins, steroids, and flavonoids tested positive in the CRE, EAF, and AQF while alkaloids were present in only the EAF. The properties of the solvent employed during extraction and fractionation influence the type of phytochemical extracted [52]. In our study, the partitioning of the alkaloids in the EAF might be due to the high affinity of the alkaloids towards ethyl acetate. Additionally, previous studies reported similar results [53, 54].

3.2. GC-MS

Table 4 presents the compounds detected by GC-MS in the EAF of DM. Grandiflorenic acid (25.36%) and dehydroabietic acid (16.09%) were the most abundant of the 59 detected compounds, next to squalene (5.36%). Moreover, Figures 1 and 3 respectively show the structural formula and the GC-MS chromatogram of the identified compounds in EAF.

The compounds identified in the AQF of DM are shown in Table 5. *Cis, cis*-linoleic acid (27.13%), and 9,17-Octadecadienal (18.88%) were detected

Table 1. List of top docked compounds with their designation and PubChem ID

Compounds	Designation	PubChem ID
5-Hydroxy-p-mentha-1,4-diene-3,6-dione	I	543659
cis-Z-. alpha. -Bisabolene epoxide	II	91753574
Diazoprogesterone	III	104633
trans-Z-. alpha. -Bisabolene epoxide	IV	5363099
Caryophyllene oxide	V	1742210

Table 2. List of the docking targets with their RSCB ID

Targets		RSCB ID	Grid box coordinates		
			X	Y	Z
Antioxidant activity	Xanthine Oxidase (XO)	3NVZ	23.19	-16.27	35.78
	Myeloperoxidase (MPO)	7LAL	19.14	-13.78	-4.43
Antidiabetic activity	11-beta-Hydroxysteroid dehydrogenase (HSD1)	3D3E	7.20	39.23	-7.88
	Sirtuin 6 (SIRT6)	6QCJ	-28.65	21.21	13.65

Table 3. Phytochemical composition of DM stembark

Phytochemical	CRE	EAF	AQF
Alkaloids	-	+	-
Saponins	+	+	+
Steroids	+	+	+
Glycosides	-	-	-
Terpenoids	-	-	-
Flavonoids	+	+	+

+ = present, - = absent.

abundantly among the 40 compounds while 3-methoxycyclohexene (0.01%) was the least abundant. Additionally, Figures 2 and 3 respectively present the structures and GC-MS chromatogram of the identified compounds in AQF. The detection and abundance of compounds in a solvent can be influenced by their affinity towards the solvent [52]. In our study, some phytochemicals were detected in different ratios between the two fractions while others were present in only one fraction which might be attributed to the solvent affinity during partitioning.

3.3. Antioxidant activity

3.3.1. Total reducing power (TRP)

The AA calibration curve and TRP of the CRE, EAF, and AQF are shown in Figure 4. The CRE, EAF, and AQF weren't significantly ($p > 0.05$) different. However, the AQF (130.83 ±1.12 mg AAE/g extract) demonstrated a slightly higher TRP than EAF (120.54 ±9.40 mg AAE/g extract) and CRE (111.03 ±5.98 mg AAE/g extract). The TRP reported here is regarded as a measure of the ability of the compounds present

ISSN: 2458 - 8806

Table 4. Identified compounds from the EAF of DM

S/N	Name	RT	Area (%)	MW	Formula
1	2,3-Dimethylpentane	4.87	0.01	100.20	C_7H1_6
2	2,2-Dimethyl-1,3-butanediol	4.97	0.01	118.17	$C_6H_{14}O_2$
3	sec-Butyl Bromide	5.06	0.02	137.02	C_4H_9Br
4	4,4-Dimethyl-cyclohex-1-enecarbonitrile	5.23	0.02	135.21	$C_9H_{13}N$
5	4-Methyl-1-hexene	5.31	0.02	98.19	C_7H_{14}
6	Caryophyllene	7.26	0.35	204.35	$C_{15}H_{24}$
7	Methyl 2-allyl-2-cyclopropene-1-carboxylate	7.51	0.01	138.16	$C_8H_{10}O_2$
8	Santolina triene	7.59	0.04	136.23	$C_{10}H_{16}$
9	4-Cyclopropylnorcarane	7.85	0.01	136.23	$C_{10}H_{16}$
10	Preg-4-en-3-one, 17. alpha-hydroxy-17. beta.-cyano-	7.88	0.01	313.4	$C_{20}H_{27}NO_2$
11	Bicyclo[4.1.0]heptane,-3-cyclopropyl,-7-hydroxymethyl, trans	7.96	0.03	166.26	$C_{11}H_{18}O$
12	γ-Muurolene	8.13	0.11	204.35	$C_{15}H_{24}$
13	Caparratriene	8.46	0.02	206.37	$C_{15}H_{26}$
14	3,6-Nonadienal, (Z,Z)	8.66	0.63	138.21	$C_9H_{14}O$
15	3-Heptyne	8.87	0.15	96.17	C_7H_{12}
16	cis-p-mentha-1(7),8-dien-2-ol	9.12	0.03	152.23	$C_{10}H_{16}O$
17	α-Limonene diepoxide	9.27	0.05	168.23	$C_{10}H_{16}O_2$
18	Diazoprogesterone	9.38	0.09	40.50	$C_{21}H_{28}N_2O_2$
19	trans-Z-.alpha.-Bisabolene epoxide	9.45	0.06	220.35	$C_{15}H_{24}O$
20	cis-Z-.alpha.-Bisabolene epoxide	9.59	0.07	220.35	$C_{15}H_{24}O$
21	(1R)-2,6,6-Trimethylbicyclo[3.1.1]hept-2-ene	9.92	0.08	136.23	$C_{10}H_{16}$
22	Elemene	10.09	0.05	204.35	$C_{15}H_{24}$
23	Cyclopentadecanone	10.15	0.20	224.38	$C_{15}H_{28}O$
24	1,12-Di(oxiran-2-yl)dodecane	10.34	0.07	254.41	$C_{16}H_{30}O_2$
25	Stearyl bromide	10.43	0.09	333.39	$C_{18}H_{37}Br$
26	Methyl palmitate	10.60	0.37	270.45	$C_{17}H_{34}O_2$
27	11,13-Dimethyl-12-tetradecenyl acetate	10.86	0.18	282.5	$C_{18}H_{34}O_2$
28	Aspidospermidin-17-ol, 1-acetyl-19,21-epoxy-15,16-dimethoxy-	10.95	0.17	414.5	$C_{23}H_{30}N_2O_5$
29	Ergost-5,8(14)-dien-3-ol	11.07	0.27	398.7	$C_{28}H_{46}O$
30	Caryophylene oxide	11.35	1.12	220.35	$C_{15}H_{24}O$

S/N	Name	RT	Area (%)	MW	Formula
31	Palmitoleic acid	11.49	1.17	254.41	$C_{16}H_{30}O_2$
32	Cyclotriacontane	11.61	0.92	420.80	$C_{30}H_{60}$
33	13-tetradecenyl acetate	12.00	3.52	254.41	$C_{16}H_{30}O_2$
34	Hentriacontane	12.10	1.56	436.84	$C_{31}H_{64}$
35	Eicosane	12.14	3.53	282.55	$C_{20}H_{42}$
36	Docosane	12.40	4.72	310.60	$C_{22}H_{46}$
37	17-Pentatriacontene	12.80	1.19	490.93	$C_{35}H_{70}$
38	(Z)-14-Tricosenyl formate	12.93	1.72	366.6	$C_{24}H_{46}O_2$
39	Dotriacontyl pentafluoropropionate	12.99	0.98	612.90	$C_{35}H_{65}F_5O_2$
40	Pentadec-7-ene, 7-bromomethyl-	13.04	0.47	303.32	$C_{16}H_{31}Br$
41	cis-Oleic Acid	13.19	3.13	282.46	$C_{18}H_{34}O_2$
42	Docos-1-ene	13.28	0.56	308.58	$C_{22}H_{44}$
43	Dehydroabietic acid	13.76	16.09	300.44	$C_{20}H_{28}O_2$
44	Grandiflorenic acid	13.93	25.36	300.4	$C_{20}H_{28}O_2$
45	1-Chlorononadecane	15.23	4.32	302.97	$C_{19}H_{39}Cl$
46	1,22-Dibromodocosane	15.44	0.39	468.4	$C_{22}H_{44}Br_2$
47	Pentadecyl 6-bromohexanoate	16.03	2.58	405.5	$C_{21}H_{41}BrO_2$
48	Squalene	16.54	5.36	410.72	$C_{30}H_{50}$
49	2-Methyl-cis-7,8-epoxynonadecane	17.08	0.19	296.5	$C_{20}H_{40}O$
50	3-Eicosene, (E)-	17.10	0.43	280.53	$C_{20}H_{40}$
51	trans-13-Octadecenoic acid	17.25	0.50	282.46	$C_{18}H_{34}O_2$
52	Trifluoroacetoxy hexadecane	17.44	0.62	338.45	$C_{18}H_{33}F_3O_2$
53	Heptacosane, 1-chloro-	17.92	4.09	415.18	$C_{27}H_{55}Cl$
54	Octadecane, 1-(methylthio)-	18.32	0.11	300.59	$C_{19}H_{40}S$
55	2-hexadecylicosanol	18.35	0.15	522.97	$C_{36}H_{74}O$
56	Malonic acid, 2,4-dimethylpent-3-yl tridecyl ester	18.39	1.44	384.60	$C_{23}H_{44}O4$
57	Trichlorooctadecylsilane	19.31	0.56	387.93	$C_{18}H_{37}Cl_3Si$
58	Tricosane	19.81	4.01	324.63	$C_{23}H_{48}$
59	9,19-Cyclolanostan-3-ol, 24,24-epoxymethano-, acetate	20.86	0.03	498.8	$C_{33}H_{54}O_3$

RT= Retention time, MW= Molecular weight.

ISSN: 2458 - 8806

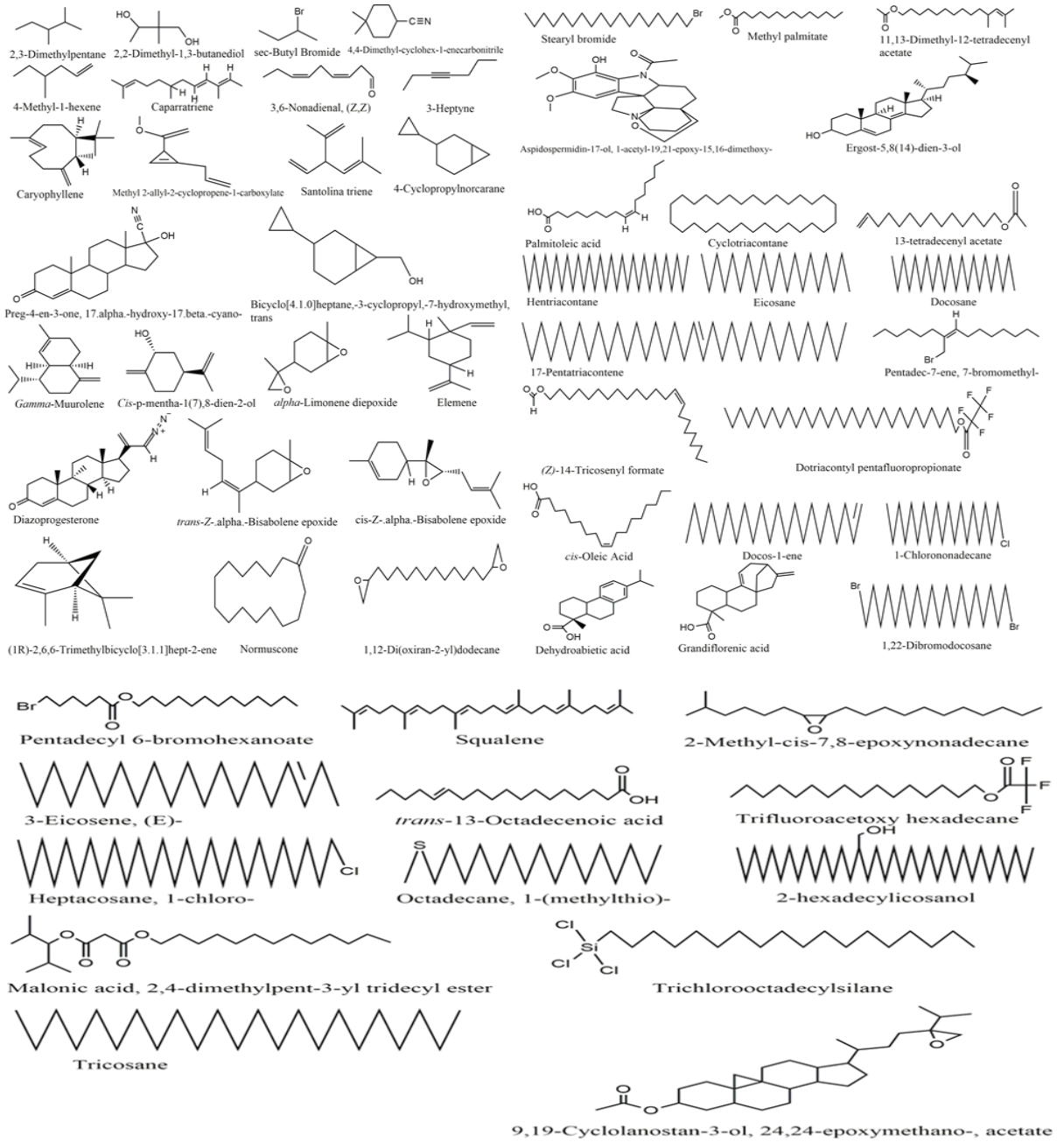

Figures 1. The structural formula of the identified compounds in EAF

in the extract to reduce ferric ions which directly reflects their potential to mitigate oxidative stress and effectively scavenge free radicals [55]. Thus, the higher reducing power of the extracts indicates potential effectiveness in reducing oxidative stress and therapeutic application in oxidative stress-linked ailments. This might be attributed to the reusability of the compounds from the extracts, acting as primary and secondary antioxidants electron donors. Therefore, they can reduce oxidized radicals multiple times [7]. Additionally, the secondary antioxidants might further enhance the activity of the primary antioxidants *via* synergistic effects [56].

3.3.2. Total antioxidant capacity (TAC)

Figure 4 presents the AA calibration curve and the TAC of the CRE, EAF, and AQF. The EAF exhibited a significantly ($p < 0.05$) higher TAC (77.78 ±0.01

Table 5. Identified Compounds from the AQF of DM

S/N	Name	RT	Area (%)	MW	Formula
1	Threitol	4.58	0.04	122.12	$C_4H_{10}O_4$
2	Maltol	4.88	0.76	126.11	$C_6H_6O_3$
3	4-Fluorobenzyl alcohol	4.92	0.19	126.13	C_7H_7FO
4	1-Ethyl-3-methylcyclohexane	4.94	0.14	126.24	C_9H_{18}
5	1-Ethyl-4-methylcyclohexane	5.04	0.83	126.24	C_9H_{18}
6	5-Ethyl-4-methyl-5-hepten-3-one	6.13	0.04	154.25	$C_{10}H_{18}O$
7	5-Hydroxy-p-mentha-1,4-diene-3,6-dione	6.17	0.04	180.20	$C_{10}H_{12}O_3$
8	3-Methoxycyclohexene	7.46	0.01	112.17	$C_7H_{12}O$
9	(1-Allylcyclopropyl) methanol	7.55	0.02	112.17	$C_7H_{12}O$
10	2-Hexyn-1-ol	7.70	0.06	98.14	$C_6H_{10}O$
11	2,5-dihydro-3-methylfurane	7.74	0.03	84.12	C_5H_8O
12	Methallyl 2-nitrophenyl ether	7.82	0.02	193.20	$C_{10}H_{11}NO_3$
13	Methyl 3-O-acetyl-beta-D-ribopyranoside	8.36	0.05	206.19	$C_8H_{14}O_6$
14	Methylmannoside	8.38	0.06	194.18	$C_7H_{14}O_6$
15	5-Fluoro-6-methyl-5-hepten-2-one	8.47	0.01	144.19	$C_8H_{13}FO$
16	Methyl b-D-Ribofuranoside	9.08	0.02	164.16	$C_6H_{12}O_5$
17	Tetrahydroactinidiolide	9.35	0.10	182.26	$C_{11}H_{18}O_2$
18	1-Methyl-3,3-pentamethylenediaziridine	9.45	0.07	126.20	$C_7H_{14}N_2$
19	Melezitose	9.47	0.04	504.4	$C_{18}H_{32}O_{16}$
20	Methyl 6-O-sec-butylhexopyranoside	9.59	0.09	250.29	$C_{11}H_{22}O_6$
21	9-Hydroxy-2,2-dimethyl-dec-5-en-3-one	9.63	0.03	198.30	$C_{12}H_{22}O_2$
22	α-D-Glucose	9.65	0.02	180.16	$C_6H_{12}O_6$
23	Altronic acid	9.71	0.08	196.16	$C_6H_{12}O_7$
24	Maltose	9.80	0.01	342.30	$C_{12}H_{22}O_{11}$
25	silver caprylate	9.83	0.01	251.07	$C_8H_{15}AgO_2$
26	Pentadecanoic acid, 14-methyl-, methyl ester	10.43	4.07	270.45	$C_{17}H_{34}O_2$
27	1-(4-Bromobutyl)-2-piperidinone	10.85	0.02	234.13	$C_9H_{16}BrNO$
28	n-Hexadecanoic acid	11.73	11.33	256.42	$C_{16}H_{32}O_2$
29	9,12-Octadecenoic acid, methyl ester	12.12	11.52	294.47	$C_{19}H_{34}O_2$

ISSN: 2458 - 8806

S/N	Name	RT	Area (%)	MW	Formula
30	Methyl stearate	12.34	6.47	298.50	$C_{19}H_{38}O_2$
31	Dimethyl 4-O-methylhexopyranosiduronate	12.57	0.40	236.22	$C_9H_{16}O_7$
32	Dioxane hydroperoxide	12.63	0.76	120.10	$C_4H_8O_4$
33	Ethyltrimethylsilane	12.69	1.02	102.25	$C_5H_{14}Si$
34	2-Pentanol, 4-methyl-, acetate	12.74	0.77	144.21	$C_8H_{16}O_2$
35	9,17-Octadecadienal	13.31	18.88	264.45	$C_{18}H_{32}O$
36	cis,cis-Linoleic acid	13.74	27.13	280.4455	$C_{18}H_{32}O_2$
37	2-Methyl-Z, Z-3,13-octadecadienol	15.20	0.28	280.50	$C_{19}H_{36}O$
38	1,12-Di(oxiran-2-yl) dodecane	15.23	0.64	254.41	$C_{16}H_{30}O_2$
39	Glyceryl Monooleate	17.84	0.18	356.54	$C_{21}H_{40}O_4$
40	2-Monoolein	17.87	1.44	356.50	$C_{21}H_{40}O_4$

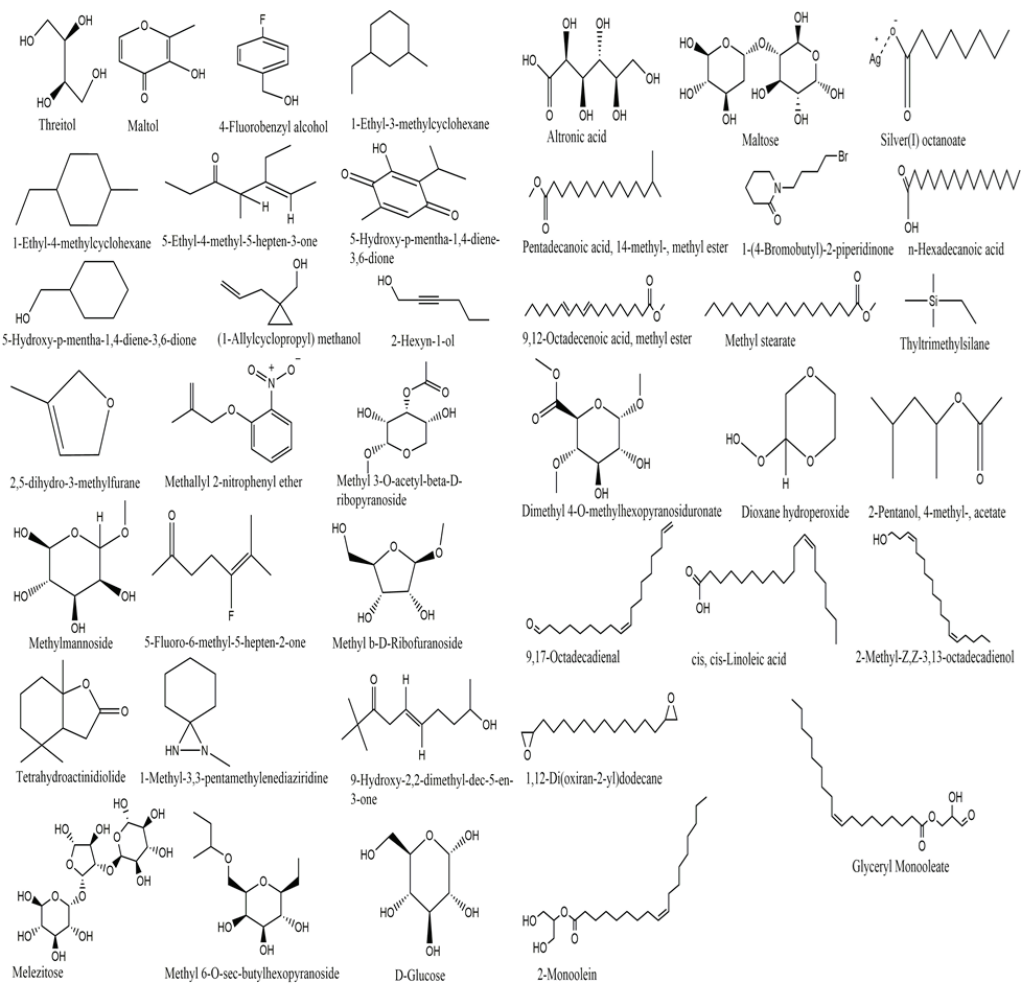

Figures 2. Structures of the identified compounds in AQF

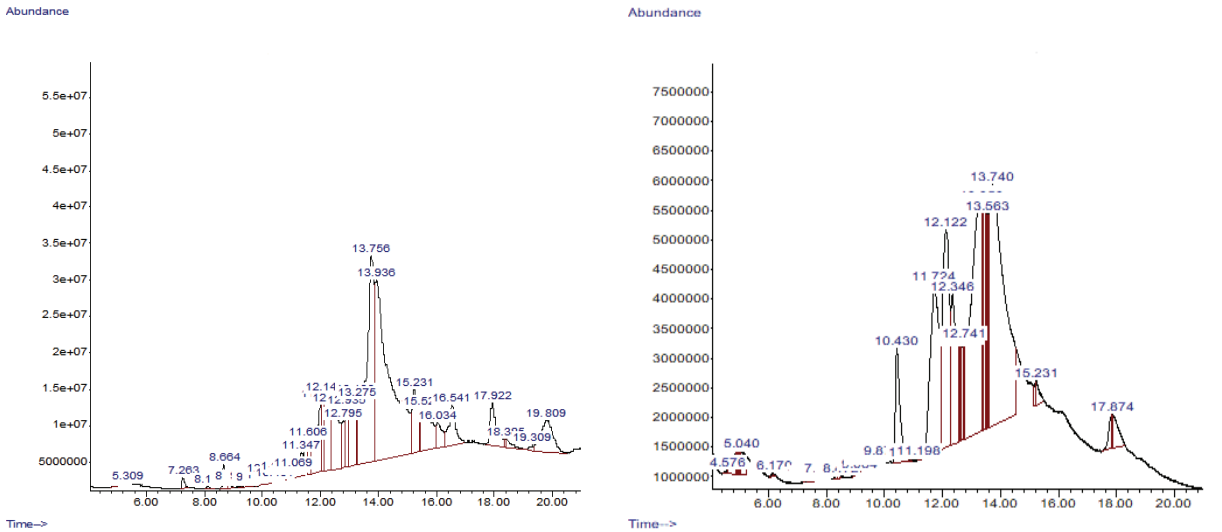

a) b)

Figure 3. GC-MS chromatogram of compounds identified in the: a) EAF and b) AQF of DM

mg AAE/g extract) than the AQF (29.63 ±0.01 mg AAE/g extract). Furthermore, the TAC of the CRE (60.20 ±0.01 mg AAE/g extract) was significantly ($p < 0.05$) higher compared to the AQF. The superior TAC exhibited by the EAF might be attributed to the presence of compounds that are absent or lower in concentration in the other fractions. Furthermore, AA exhibited superior activity here which might be attributed to its strong antioxidant activity [57]. Similar to the TRP, the TAC evaluates the potential of the extracts to neutralize free radicals and mitigate oxidative damage associated with oxidative stress-linked conditions [58]. Thus, based on our report, the EAF might demonstrate superior activity against oxidative stress than its counterparts.

3.3.3. FTC method

Figure 4 displays the lipid peroxidation inhibitory activity of the CRE, EAF, and AQF by the FTC method. The EAF (38.27% ±2.44) and AA (32.26% ±3.12) demonstrated significantly ($p < 0.05$) higher percentage inhibition than CRE (17.45% ±2.18) and AQF (15.91% ±2.11). The FTC method defines the activity of the extracts against the early stage of lipid peroxidation where decreased absorbance levels indicate higher activity [59]. In our study, the EAF exhibited the highest percentage of inhibition and thus, the highest activity. Moreover, the hydrophobic medium of the FTC method might further favor the activity of the EAF than the other extracts. Lipid peroxidation is minimized in the presence of antioxidants with anti-peroxidation effects. This preserves membrane integrity, cellular components, and enzyme activities by scavenging free radicals, mitigating their effects and preventing oxidative stress-linked ailments [60].

3.3.4. TBA method

Figure 4 presents the lipid peroxidation inhibitory activity of the CRE, EAF, and AQF *via* the TBA method. The lowest MDA concentration was exhibited by the CRE (0.71 ±0.02 nmol/ml), next to EAF (0.74 ±0.02 nmol/ml) and AQF (0.87 ±0.01 nmol/ml). Moreover, all the extracts had significantly ($p < 0.05$) lower MDA concentrations than AA (0.83 ±0.02 nmol/ml). The TBA method defines the antioxidant activity by depicting the capacity to prevent MDA formation, a secondary product of lipid peroxidation from peroxides [61]. The CRE demonstrated a slightly superior activity in the TBA method, thus a higher anti-lipid peroxidation.

3.3.5. Hydrogen peroxide scavenging assay

Figure 4 shows the H_2O_2 scavenging activity of the CRE, EAF, and AQF. All the extracts demonstrated significantly ($p < 0.05$) higher scavenging potential against AA at 20 and 60 µg/ml concentrations. However, only the CRE and AQF exhibited higher potential than AA at 80 and 100 µg/ml. Additionally, the EAF exhibited a significant ($p < 0.05$) decrease

ISSN: 2458 - 8806

in activity than AQF at 100 µg/ml. The extract's peroxide scavenging potential was explored in this assay and the AQF exhibited the highest peroxide scavenging potential, further demonstrating the anti-lipid peroxidation effects and reducing potential of the extract.

3.4. In silico study

3.4.1. MD and MDS

Exactly 33 compounds passed Lipinski's rule and Veber's filter which were docked with the target proteins. The docking interactions of the targets with the compounds are shown in Table 6. The lowest BA (-9 kcal/mol) and Ki (0.25 µM) were exhibited by III, interacting with MPO. Moreover, 10 HBIs were formed, in addition to a salt bridge interaction with Asp94. However, compound I had 2 HBs, absent in III. Furthermore, this compound (III) exhibited the lowest BA (-9.9 kcal/mol) and Ki (0.05 µM) with superior HBs (3), interacting with XO. However, IV exhibited higher HBIs (11) than III.

Compound III exhibited the lowest BA (-10 kcal/mol) and Ki (0.05 µM) with more HBs (3) and HBIs (9), demonstrating the most favorable docking interaction with HSD1. Furthermore, it exhibited the least BA (-10 kcal/mol) and Ki (0.05 µM) with SIRT6, similar to the result of the HSD1. Moreover, it had the highest number of HBs (3) and HBIs (9).

Figure 8 reveals the 2D and 3D docking interaction of the targets with III, depicting the HBs and HBIs including HB distances. The interaction of III with MPO showed docking in a hydrophobic pocket without HB interaction. Three HBs with Gly260, Val259, and Pro400 were exhibited by XO, interacting with III with bond distances of 3.26, 3.10, and 3.23 Å, respectively. Furthermore, HSD1 interaction showed HB binding with III including a double with Lys44 with distances of 3.01 and 3.17 Å, in addition to a 3.25 Å with Gly41. Lastly, a HB with Ser216 (2.93 Å) was formed by SIRT6 with III.

Figure 6 reveals the MDS of the apo and III-docked MPO, showing the fluctuation of residues and clusters. The MDS of the docked MPO showed increased residues and cluster displacements compared to the apoMPO with the highest by Ser42 (5.14 Å) at the N-terminal cluster, next to Gly121 (3.75 Å). Moreover, Gly351 close to the midchain showed higher RMSF (3.59 Å) while Asn549 fluctuated (2.83 Å) at the C-terminal. MPO is an important enzyme in inflammatory and oxidative stress conditions, making it a target of conditions accompanied by a rise in oxidative stress like diabetes [62]. It promotes reactive oxygen and nitrogen species generation and one such reaction is the reaction between H_2O_2 with Cl to yield HOCl [62]. Therefore, inhibiting its enzyme activity might decrease ROS generation and oxidative stress. Moreover, Glu242 and Asp94 were reported to be involved in the stability and catalysis of the enzyme [63]. In our study, compound III exhibited the lowest BA and Ki while interacting with MPO, involving Glu242 and Asp94 with the MDS showing residues and cluster displacements within the enzyme. This could lead to a possible disruption of its structural integrity and activity.

Table 6. Docking interactions of the targets with the compounds

Targets	Compounds	BA (kcal/mol)	Ki (µM)	HB	HBI	Salt Bridge
MPO	III	-9	0.25	-	10	Asp94
	I	-7	7.3	2	8	
XO	III	-9.9	0.05	3	7	
	IV	-7.7	2.24	-	11	
HSD1	III	-10	0.05	3	9	
	V	-7.5	3.14	-	6	
SIRT6	III	-10	0.05	1	9	
	V	-7.7	2.24	-	8	

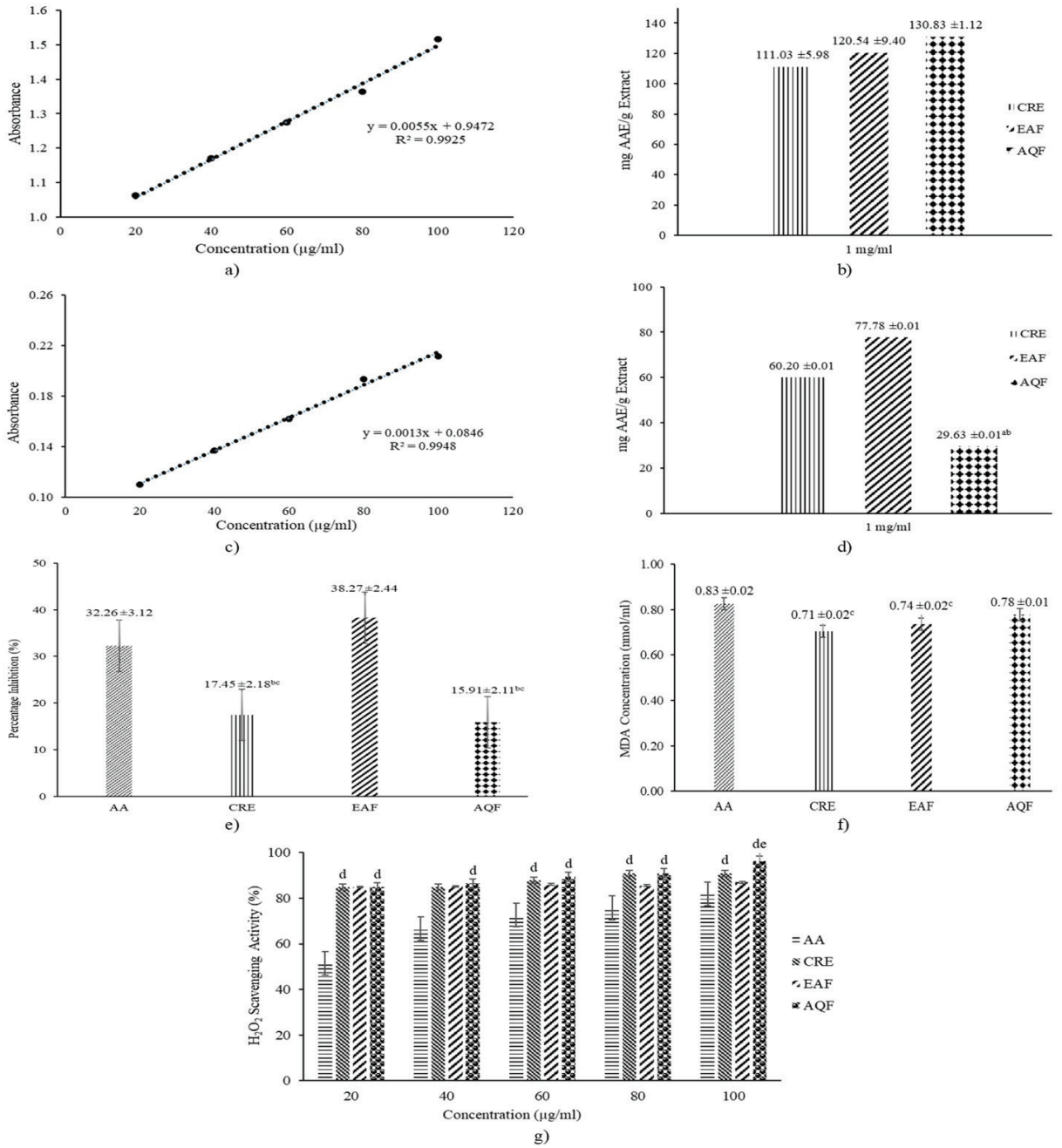

Figure 4. Antioxidant activity of CRE, EAF, and AQF; a) AA calibration curve of TRP, b) TRP, c) AA calibration curve of TAC, d) TAC, e) FTC, f) TBA, and g) H_2O_2 scavenging. Values with [a, b,] and [c] superscripts are significantly ($p < 0.05$) lower than CRE, EAF, and AA, respectively. Values with [d] and [e] superscripts are significantly ($p < 0.05$) higher than AA and EAF, respectively

The MDS of the apo and docked XO complex is displayed in Figure 6, showing a compared residue and cluster displacements. Notably, higher displacement of residues in the docked complex was observed at the tail terminal cluster and residue (Cys1325; 8.96 Å), next to Glu133 at the N-terminal. Gly502 (3.56 Å) fluctuated close to the midchain while Pro253 (2.94 Å) and Thr853 (3.11 Å) were on either side of the midchain. XO is vital to purine catabolism, catalyzing the conversion of hypoxanthine to xanthine and then uric acid [64]. Moreover, this enzyme generates reactive oxygen and nitrogen species in addition to superoxide ions [64]. In conditions like diabetes where there is excess free radicals' generation and

ISSN: 2458 - 8806

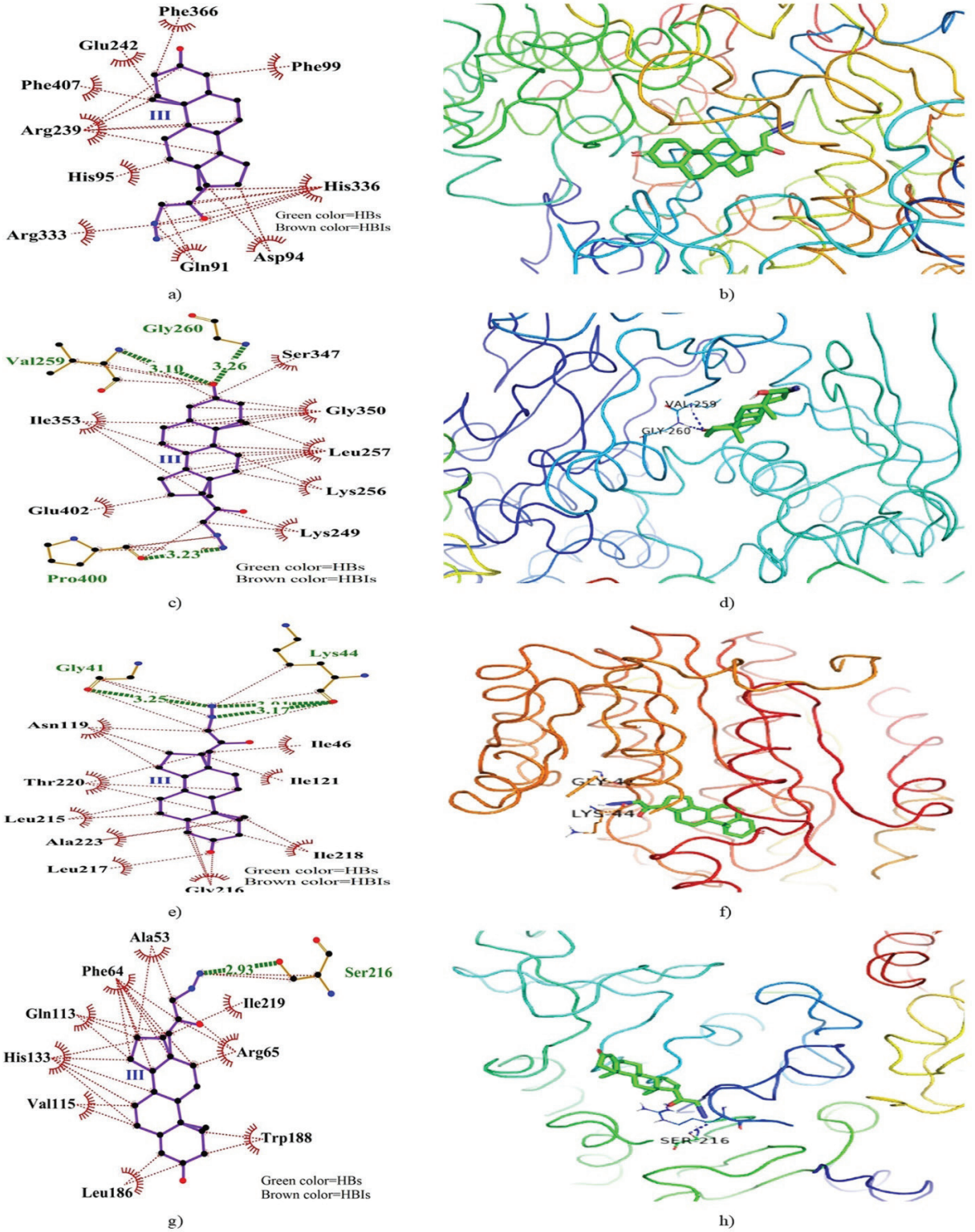

Figure 5. 2D and 3D dock poses of III, respectively with MPO (a and b), XO (c and d), HSD1 (e and f), and SIRT6 (g and h)

depletion of the antioxidant systems, minimizing or inhibiting XO activity might prove to be vital. Moreover, Glu802, Arg880, and Glu1261 were previously identified as active site residues of XO, significantly affecting substrate attachment, rate of reaction, and proton transfer, respectively [65]. In our study, compound III interacted with XO with the lowest BA which might lead to the disruption of its activity. Moreover, the MDS also revealed residues and cluster displacements of its structure.

The MDS result depicting the cluster and RMSF of the undocked and compound III-docked HSD1 is presented in Figure 6. Ser281 (7.71 Å) at the C-terminal cluster was the most fluctuated among the residues compared to the apoenzyme with Glu21 (2.83 Å) and Ala42 (2.05 Å) fluctuated at the N-terminal. Moreover, Leu126 (3.30 Å) and Pro178 (1.41 Å) close to the midchain fluctuated higher compared to the apo counterpart. HSD1 catalyzed the conversion of cortisone to cortisol, the active form where its accumulation promotes insulin resistance and subsequent hyperglycemia [66]. This enzyme is regarded as a potential therapeutic target for type 2 diabetes antidiabetic drugs [66]. Furthermore, Gly216 and Ile218 were previously identified as active site residues of the enzyme and a potential target of inhibition [67]. In our study, Ile218 and Gly216 were involved in HBI with HSD1 in addition to the low BA and Ki interaction which might disrupt its tertiary structure and its activity. This is further supported by the MDS result of the docked complex, showing a high displacement of clusters and residues.

The MDS result of the III-docked SIRT6 complex is presented in Figure 6, depicting the cluster and residue fluctuations. Leu78 (3.91 Å) appears to be highly fluctuated compared to the apoenzyme at the N-terminal while Pro290 (3.54 Å) fluctuated at the C-terminal. Furthermore, Cys177 (3.48 Å), Lys143 (2.43 Å), and Glu189 (2.99 Å) were notably fluctuated at close to midchain while Lys15 (3.10 Å) and Ala275 (3.27 Å) at the N- and C-terminals, respectively. SIRT6 has been recently identified as a nuclear protein that promotes insulin secretion and inhibits liver gluconeogenesis, adiposity, and triglyceride synthesis. Thus, an important target for its modulators as antidiabetic therapeutics [68]. However, recent studies showed that a deficiency of SIRT6 improves glucose uptake by tissues and promotes the expression of glycolytic enzymes, attenuating hyperglycemia [19]. Moreover, Phe64, Val115, His133, and Trp188 were previously identified as the active site residues of SIRT6 [69]. In our study, the interaction of compound III with SIRT6 involved these active site residues. Moreover, the lowest BA and Ki exhibited by the III-docked SIRT6 might inhibit its activity and improve glucose metabolism. Furthermore, the MDS showed high residue and cluster displacement, further supporting the disruption of its tertiary structure and possible activity.

3.4.2. ADMET predictions

The ADMET predictions of the best-docked compound (III) are displayed in Table 7, depicting its predicted ADMET properties. Compound III was predicted to be less soluble in water (-4.99 log mol/L) with high intestinal absorption (99%) in humans. Additionally, the skin permeability was -2.99 log Kp. A skin permeability value > -2.5 log Kp is considered low [51]. Thus, compound III has high skin permeability. Moreover, it was predicted as a P-glycoprotein substrate and inhibitor of P-glycoprotein I. The P-glycoprotein acts as a barrier by extruding toxins and xenobiotics out of the cell and its inhibition might result in adverse effects and contradictions [51]. The steady-state volume of distribution (VDss) of III was 0.51 log L/kg with a fraction unbound value of 0.07. A VDss value of < -0.15 log L/kg is considered low while > 0.45 log L/kg is high. A fraction unbound translates to the number of drugs available for cellular entry which affects its efficacy [51]. Thus, III was predicted to have high VDss with low efficacy. The predicted blood-brain barrier (BBB) and central nervous system (CNS) permeability values of compound III were 0.07 log BB and -1.64 log PS, respectively. A compound with log BB > 0.3 and log PS > -2 is considered BBB and CNS permeant, respectively while log BB < -1 and log PS < -3 are poorly BBB permeant and non-CNS penetrant, respectively [51]. Thus, the compound was predicted to be non-BBB but CNS permeant.

Compound III was predicted to be substrate and non-substrate of CYP3A4 and CYP2D6, respectively. Moreover, it is a non-inhibitor of CYP1A2, CYP2C19, CYP2C9, CYP2D6, and CYP3A4. The cytochrome P450 enzymes are responsible for the detoxification of drugs mostly in the liver, thereby, affecting drug pharmacokinetics [51]. Additionally, the compound was predicted to have low renal clearance (0.01 log ml/min/kg) and a non-substrate of renal organic

ISSN: 2458 - 8806

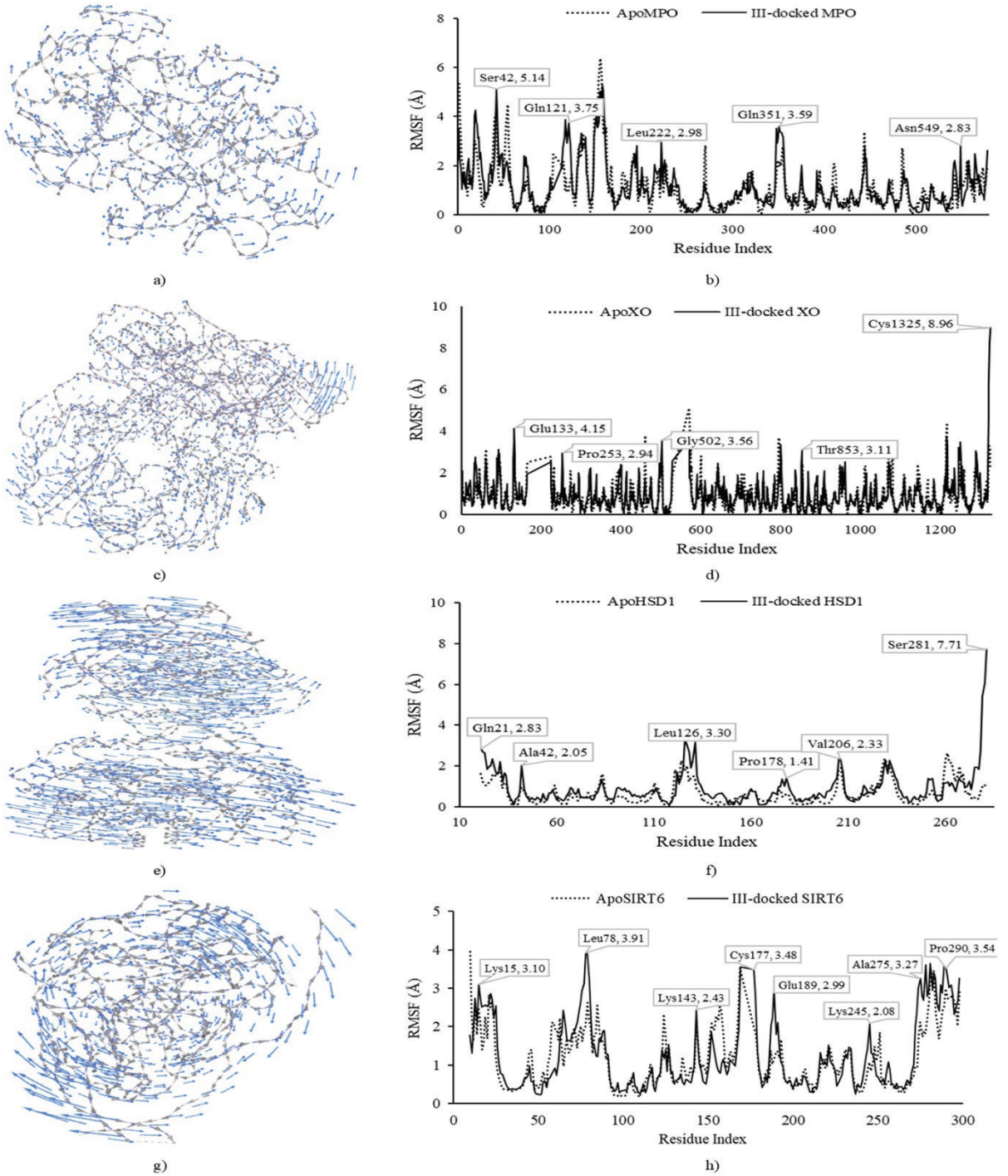

Figure 6. MDS of apo and III-docked targets, showing the respective cluster and RMSF of; MPO (a and b), XO (c and d), HSD1 (e and f), and SIRT6 (g and h)

cation transporter 2 (OCT2) which performs renal clearance and disposition of drugs [51]. The toxicity prediction of compound III showed a maximum tolerable (human) of -0.89 log mg/kg/day and a non-inhibitor and inhibitor of hERG I and II, respectively. A maximum tolerable dose <= 0.477 log (mg/kg/day) and above is considered low and high, respectively. Thus, compound III has a low maximum tolerable

dose. Additionally, the compound was predicted to have LD_{50} of 2.37 mol/kg in rats and hepatoxic without skin sensation.

4. Conclusion

DM exhibited strong antioxidant and antidiabetic potential that might be due to the identified compounds which is supported by the observed free radical scavenging and *in-silico* interactions of the compounds with the antidiabetic and antioxidant targets. Moreover, the *in vitro* antioxidant study correlates with the *in silico* as diazoprogesterone (Compound III) identified in the EAF exhibited superior antioxidant activity. Additionally, the identified compounds might be a source of novel therapeutics against oxidative stress and diabetes which might be achieved *via* structural modifications.

Acknowledgments

The authors express their gratitude to the Tertiary Education Trust Fund of Nigeria for sponsoring this research through the Institutional Based Research Fund of Adamawa State Polytechnic, Yola. A special appreciation also goes to the Pharmaceutical Technology Department for institutional support.

Table 7. ADMET predictions of diazoprogesterone (Compound III)

	ADMET Properties	Compound III
Absorption	Water solubility (log mol/L)	-4.99
	Human Intestinal absorption (%)	98.00
	Skin permeability (log Kp)	-2.99
	P-glycoprotein substrate	No
	P-glycoprotein I inhibitor	Yes
	P-glycoprotein II inhibitor	No
Distribution	The volume of distribution [VDss (log L/kg)]	0.51
	Human fraction unbound	0.07
	BBB permeability (log BB)	0.07
	CNS permeability (log PS)	-1.64
Metabolism	CYP2D6 substrate	No
	CYP3A4 substrate	Yes
	CYP1A2 inhibitor	No
	CYP2C19 inhibitor	No
	CYP2C9 inhibitor	No
	CYP2D6 inhibitor	No
	CYP3A4 inhibitor	No
Excretion	Total clearance (log ml/min/kg)	0.01
	Renal OCT2 substrate	No
Toxicity	Human max. tolerated dose (log mg/kg/day)	-0.89
	hERG I inhibitor	No
	hERG II inhibitor	Yes
	LD50 [rats (mol/kg)]	2.37
	Hepatotoxicity	Yes
	Skin sensation	No

ISSN: 2458 - 8806

Conflict of Interest

The author has no conflicts of interest, financial or otherwise to declare.

Statement of Contribution of Researchers

Concept: M. M. D., N. M.; Design: M. M. D., N. M Control: M. M. D., N. M.; Sources: M. M. D.; Materials: M. M. D., N. M.; Data Collection and/or Processing: M. M. D., N. M.; Analysis and/or Interpretation: M. M. D., N. M.; Literature Review: M. M. D.; Manuscript Writing: M. M. D..; Critical Review: M. M. D., N. M.

References

1. American Diabetes Association Professional Practice Committee. Classification and Diagnosis of Diabetes: Standards of Medical Care in Diabetes—2022. Diabetes Care. 2022;45(1):S17-S38. https://doi.org/10.2337/dc22-s002
2. Bhatti JS, Sehrawat A, Mishra J, Sidhu IS, Navik U, Khullar N, et al. Oxidative stress in the pathophysiology of type 2 diabetes and related complications: Current therapeutics strategies and future perspectives. Free Radical Biol Med. 2022;184:114-34. https://doi.org/10.1016/j.freeradbiomed.2022.03.019
3. Domingueti CP, Dusse LMSA, Carvalho MdG, de Sousa LP, Gomes KB, Fernandes AP. Diabetes mellitus: The linkage between oxidative stress, inflammation, hypercoagulability and vascular complications. J Diabetes Complications. 2016;30(4):738-45. https://doi.org/10.1016/j.jdiacomp.2015.12.018
4. Giacco F, Brownlee M. Oxidative stress and diabetic complications. Circul Res. 2010;107(9):1058-70. https://doi.org/10.1161/circresaha.110.223545
5. Pasupuleti VR, Arigela CS, Gan SH, Salam SKN, Krishnan KT, Rahman NA, et al. A Review on Oxidative Stress, Diabetic Complications, and the Roles of Honey Polyphenols. Oxid Med Cell Longev. 2020;2020:8878172. https://doi.org/10.1155/2020/8878172
6. Adwas AA, Elsayed A, Azab AE, Quwaydir FA. Oxidative stress and antioxidant mechanisms in human body. J Appl Biotechnol Bioeng. 2019;6(1):43-7. https://doi.org/10.15406/jabb.2019.06.00173
7. Ali SS, Ahsan H, Zia MK, Siddiqui T, Khan FH. Understanding oxidants and antioxidants: Classical team with new players. J Food Biochem. 2020;44(3):e13145. https://doi.org/10.1111/jfbc.13145
8. Hayes JD, Dinkova-Kostova AT, Tew KD. Oxidative Stress in Cancer. Cancer Cell. 2020;38(2):167-97. https://doi.org/10.1016/j.ccell.2020.06.001
9. Klaunig JE. Oxidative Stress and Cancer. Curr Pharm Des. 2018;24(40):4771-8. https://doi.org/10.2174/1381612825666190215121712
10. Abenavoli L, Milic N. Chapter 45 - Silymarin for Liver Disease. In: Muriel P, editor. Liver Pathophysiology. Boston: Academic Press; 2017. 631 p. https://doi.org/10.1016/B978-0-12-804274-8.00045-X
11. Naris S. Significant Role of Free Radicals in Diabetes Mellitus. Oxidants and Antioxidants in Medical Science. 2022;11(08):1-2.
12. Dahiru MM, Alfa MB, Abubakar MA, Abdulllahi AP. Assessment of in silico antioxidant, anti-inflammatory, and antidiabetic activites of Ximenia americana L. Olacaceae. Advances in Medical, Pharmaceutical and Dental Research. 2024;4(1):1-13. http://dx.doi.org/10.21622/AMPDR.2024.04.1.735
13. Dahiru MM, Musa N. Phytochemical Profiling, Antioxidant, Antidiabetic, and ADMET Study of *Diospyros mespiliformis* Leaf, Hochst Ex A. Dc Ebenaceae. J Fac Pharm Ankara/Ankara Ecz Fak Derg. 2024;48(2):412-35. http://dx.doi.org/10.33483/jfpau.1354293
14. Dahiru MM, Musa N, Abaka AM, Abubakar MA. Potential Antidiabetic Compounds from Anogeissus leiocarpus: Molecular Docking, Molecular Dynamic Simulation, and ADMET Studies. Borneo J Pharm. 2023;6(3):249-77. https://doi.org/10.33084/bjop.v6i3.5027
15. Heitaku S, Sasase T, Sotani T, Maki M, Katsumi S, Fukuda S, et al. An 11-beta hydroxysteroid dehydrogenase type 1 inhibitor, JTT-654 ameliorates insulin resistance and non-obese type 2 diabetes. Biol Pharm Bull. 2023;46(7):969-78. https://doi.org/10.1248/bpb.b23-00129
16. Morgan SA, Gathercole LL, Hassan-Smith ZK, Tomlinson J, Stewart PM, Lavery GG. 11β-HSD1 contributes to age-related metabolic decline in male mice. J Endocrinol. 2022;255(3):117-29. https://doi.org/10.1530/joe-22-0169
17. Wu K, Wang Y, Liu R, Rui T. The role of mammalian Sirtuin 6 in cardiovascular diseases and diabetes mellitus. Front Physiol. 2023;14:1207133. https://doi.org/10.3389/fphys.2023.1207133
18. Wang Y, Enrick M, Gadd J, Yin L. The regulatory role of Sirtuin 6 in coronary endothelial dysfunction in HFpEF. Physiology. 2023;38(S1):5733428. http://dx.doi.org/10.1152/physiol.2023.38.S1.5733428
19. Sociali G, Magnone M, Ravera S, Damonte P, Vigliarolo T, Von Holtey M, et al. Pharmacological Sirt6 inhibition improves glucose tolerance in a type 2 diabetes mouse model. The FASEB Journal. 2017;31(7):3138. https://doi.org/10.1096/fj.201601294r

20. Parenti MD, Grozio A, Bauer I, Galeno L, Damonte P, Millo E, et al. Discovery of novel and selective SIRT6 inhibitors. J Med Chem. 2014;57(11):4796-804. https://doi.org/10.1021/jm500487d

21. Yu G, Liang Y, Zheng S, Zhang H. Inhibition of myeloperoxidase by N-acetyl lysyltyrosylcysteine amide reduces oxidative stress–mediated inflammation, neuronal damage, and neural stem cell injury in a murine model of stroke. J Pharmacol Exp Ther. 2018;364(2):311-22. https://doi.org/10.1124/jpet.117.245688

22. Chen S, Chen H, Du Q, Shen J. Targeting myeloperoxidase (MPO) mediated oxidative stress and inflammation for reducing brain ischemia injury: Potential application of natural compounds. Front Physiol. 2020;11:433. https://doi.org/10.3389/fphys.2020.00433

23. Romagnoli M, Gomez-Cabrera M-C, Perrelli M-G, Biasi F, Pallardó FV, Sastre J, et al. Xanthine oxidase-induced oxidative stress causes activation of NF-κB and inflammation in the liver of type I diabetic rats. Free Radical Biol Med. 2010;49(2):171-7. https://doi.org/10.1016/j.freeradbiomed.2010.03.024

24. Dahiru MM, Nadro SM. A review of the Mechanisms of Action and Side Effects of Anti-diabetic Agents. Trends in Pharmaceutical Sciences. 2022;8(3):195-210. http://dx.doi.org/10.30476/TIPS.2022.95931.1153

25. Dahiru MM. Recent advances in the therapeutic potential phytochemicals in managing diabetes. Journal of Clinical and Basic Research. 2023;7(1):13-20. https://jcbr.goums.ac.ir/article-1-385-en.html

26. Cao S-Y, Li B-Y, Gan R-Y, Mao Q-Q, Wang Y-F, Shang A, et al. The in vivo antioxidant and hepatoprotective actions of selected Chinese teas. Foods. 2020;9(3):262. https://doi.org/10.3390%2Ffoods9030262

27. Dahiru MM, Nadro MS. Phytochemical Composition and Antioxidant Potential of Hyphaene thebaica Fruit. Borneo J Pharm. 2022;5(4):325-33. https://doi.org/10.33084/bjop.v5i4.3632

28. Dahiru MM, Ahmadi H, Faruk MU, Aminu H, Hamman, Abreme GC. Phytochemical Analysis and Antioxidant Potential of Ethylacetate Extract of Tamarindus Indica (Tamarind) Leaves by Frap Assay. Journal of Fundamental and Applied Pharmaceutical Science. 2023;3(2):45-53. https://doi.org/10.18196/jfaps.v3i2.16708

29. Musa N, Dahiru MM, Badgal EB. Characterization, In Silico Antimalarial, Antiinflammatory, Antioxidant, and ADMET Assessment of Neonauclea excelsa Merr. Sciences of Pharmacy. 2024;3(2):92-107. https://doi.org/10.58920/sciphar0302232

30. Uduwana S, Abeynayake N, Wickramasinghe I. Synergistic, antagonistic, and additive effects on the resultant antioxidant activity in infusions of green tea with bee honey and Citrus limonum extract as additives. J Agric Food Res. 2023;12:100571. https://doi.org/10.1016/j.jafr.2023.100571

31. Dahiru MM, Umar AS, Muhammad M, Fari II, Musa ZY. Phytoconstituents, Fourier-Transform Infrared Characterization, and Antioxidant Potential of Ethyl Acetate Extract of Corchorus olitorius (Malvaceae). Sciences of Phytochemistry. 2024;3(1):1-10. https://doi.org/10.58920/sciphy0301208

32. Dahiru MM, Nadro MS. Anti-diabetic potential of Hyphaene thebaica fruit in streptozotocin-induced diabetic rats. J Expl and Molec Biol. 2022;23(1):29-36. https://doi.org/10.47743/jemb-2022-63

33. Samuel NA, Koura K, Ganglo CJ. Ethnobotanical assessment of *Diospyros mespiliformis Hochst. ex A. DC* (Ebenaceae) in the classified forest of Wari-Maro (Sudano-guinean area of Benin, West Africa). Ethnobot Res Appl. 2021;22:1-12. http://dx.doi.org/10.32859/era.22.45.1-12

34. Ebbo AA, Sani D, Suleiman MM, Ahmad A, Hassan AZ. Assessment of antioxidant and wound healing activity of the crude methanolic extract of *Diospyros mespiliformis Hochst ex a. Dc* (Ebenaceae) and its fractions in Wistar rats. S Afr J Bot. 2022;150:305-12. https://doi.org/10.1016/j.sajb.2022.07.034

35. Muhammad NB, Wasagu RSU, Sani B. Effect of Methanolic Extract of African Ebony *(Diospyros mespiliformis)* Stem Bark on Liver and Kidney Function Biomarkers in Alloxan Induced Diabetic Albino Rats. Asian J Biochem Genet Mol Biol. 2020;6(3):51-5. https://doi.org/10.9734/ajbgmb/2020/v6i330156

36. Evans WC. Trease and Evans' pharmacognosy: Elsevier Health Sciences; 2009. 608 p.

37. Indumathi C, Durgadevi G, Nithyavani S, Gayathri P. Estimation of terpenoid content and its antimicrobial property in Enicostemma litorrale. Int J ChemTech Res. 2014;6(9):4264-7.

38. Dahiru MM, Badgal EB, Musa N. Phytochemistry, GS-MS analysis, and heavy metals composition of aqueous and ethanol stem bark extracts of Ximenia americana. GSC Biol Pharm Sci. 2022;21(3):145-56. http://dx.doi.org/10.30574/gscbps.2022.21.3.0462

39. Oyaizu M. Studies on products of browning reaction antioxidative activities of products of browning reaction prepared from glucosamine. The Japanese journal of nutrition and dietetics. 1986;44(6):307-15. http://dx.doi.org/10.5264/eiyogakuzashi.44.307

40. Prieto P, Pineda M, Aguilar M. Spectrophotometric quantitation of antioxidant capacity through the formation of a phosphomolybdenum complex: specific application to the determination of vitamin E. Anal Biochem. 1999;269(2):337-41. https://doi.org/10.1006/abio.1999.4019

ISSN: 2458 - 8806

41. Kikuzaki H, Nakatani N. Antioxidant effects of some ginger constituents. J Food Sci. 1993;58(6):1407-10. https://www.doi.org/10.1111/J.1365-2621.1993.TB06194.X

42. Kwon TW, Watts B. Determination of Malonaldehyde by Ultraviolet Spectrophotometry. J Food Sci. 2006;28:627-30. https://doi.org/10.1111/j.1365-2621.1963.tb01666.x

43. Zhang XY. Principles of chemical analysis. Beijing: China Science Press. 2000. 276 p.

44. Sanner MF. Python: a programming language for software integration and development. J Mol Graph Model. 1999;17(1):57-61.

45. Jendele L, Krivák R, Škoda P, Novotný M, Hoksza D. PrankWeb: a web server for ligand binding site prediction and visualization. Nucleic Acids Res. 2019;47:345-9. https://doi.org/10.1093/nar/gkz424

46. Laskowski RA, Swindells MB. LigPlot+: Multiple Ligand–Protein Interaction Diagrams for Drug Discovery. J Chem Inf Model. 2011;51(10):2778-86. https://doi.org/10.1021/ci200227u

47. Adasme MF, Linnemann KL, Bolz SN, Kaiser F, Salentin S, Haupt VJ, et al. PLIP 2021: Expanding the scope of the protein–ligand interaction profiler to DNA and RNA. Nucleic Acids Res. 2021;49(W1):W530-W4. https://doi.org/10.1093/nar/gkab294

48. Ortiz CLD, Completo GC, Nacario RC, Nellas RB. Potential Inhibitors of Galactofuranosyltransferase 2 (GlfT2): Molecular Docking, 3D-QSAR, and In Silico ADMETox Studies. Sci Rep. 2019;9(1):17096. https://doi.org/10.1038/s41598-019-52764-8

49. Tiwari SP, Fuglebakk E, Hollup SM, Skjærven L, Cragnolini T, Grindhaug SH, et al. WEBnm@ v2.0: Web server and services for comparing protein flexibility. BMC Bioinformatics. 2014;15(1):1-12. https://doi.org/10.1186/s12859-014-0427-6

50. Kurcinski M, Oleniecki T, Ciemny MP, Kuriata A, Kolinski A, Kmiecik S. CABS-flex standalone: a simulation environment for fast modeling of protein flexibility. Bioinformatics. 2019;35(4):694-5. https://doi.org/10.1093/bioinformatics/bty685

51. Pires DEV, Blundell TL, Ascher DB. pkCSM: Predicting Small-Molecule Pharmacokinetic and Toxicity Properties Using Graph-Based Signatures. J Med Chem. 2015;58(9):4066-72. https://doi.org/10.1021/acs.jmedchem.5b00104

52. Chóez-Guaranda I, Viteri-Espinoza R, Barragán-Lucas A, Quijano-Avilés M, Manzano P. Effect of solvent-solvent partition on antioxidant activity and GC-MS profile of Ilex guayusa Loes. leaves extract and fractions. Nat Prod Res. 2022;36(6):1570-4. https://doi.org/10.1080/14786419.2021.1882455

53. Ebbo AA, Sani D, Suleiman MM, Ahmed A, Hassan AZ. Phytochemical Composition, Proximate Analysis and Antimicrobial Screening of the Methanolic Extract of *Diospyros mespiliformis Hochst Ex a. Dc* (Ebenaceae). Pharmacognosy Journal. 2019;11(2):362-8. http://dx.doi.org/10.5530/pj.2019.11.55

54. Adamu HM, Yushaus YA. Phyto chemical screening and antioxidant activity of the stem bark extracts of *Diospyros mespiliformis:* a medicinal plant in Bauchi. International Journal of Pharmacy Research & Technology (IJPRT). 2023;10(1):37-43. https://doi.org/10.31838/ijprt/10.01.08

55. Hajiabdolah N, Parsa A, Anaraki-Ardakani H, Jalali-Jahromi H. Iron (III) reduction as a measure of "antioxidant power" using homo and copolymer of pyrrole and aniline electrosynthesized. Rev Roum Chim. 2020;65(3):247-54. http://dx.doi.org/10.33224/rrch.2020.65.3.04

56. Ladaniya M. Chapter 6 - Fruit biochemistry. In: Ladaniya M, editor. Citrus Fruit (Second Edition): Academic Press; 2023. 247 p. https://doi.org/10.1016/B978-0-323-99306-7.00021-9

57. Gęgotek A, Skrzydlewska E. Chapter Nine - Ascorbic acid as antioxidant. In: Litwack G, editor. Vitam Horm. 121: Academic Press; 2023. 270 p. https://doi.org/10.1016/bs.vh.2022.10.008

58. Zheng Y, Li X, Wei C, Gao Y, Han G, Zhao J, et al. Long-lived phosphorescent carbon dots as photosensitizers for total antioxidant capacity assay. Anal Chem. 2023;95(23):8914-21. https://doi.org/10.1021/acs.analchem.3c00657

59. Shafekh ES, Khalili MAR, Catherine CCW, Syakiroh SZA, Habibah UA, Norhayati AH, et al. Total phenolic content and in vitro antioxidant activity of Vigna sinensis. Int Food Res J. 2012;19(4):1393. http://dx.doi.org/10.3923/pjn.2013.416.422

60. Stankevych L, Khmelnytska Y, Ephanova V. The effect of antioxidants on lipid peroxidation in modern pentathlon athletes. Scientific Journal of National Pedagogical Dragomanov University Series 15 Scientific and pedagogical problems of physical culture (physical culture and sports). 2023;3(162):379-85. https://doi.org/10.31392/npu-nc.series15.2023.3k(162).79

61. Marín R, Abad C, Rojas D, Chiarello DI, Alejandro T-G. Chapter Four - Biomarkers of oxidative stress and reproductive complications. In: Makowski GS, editor. Adv Clin Chem. 113: Elsevier; 2023. 233 p. https://doi.org/10.1016/bs.acc.2022.11.004

62. Chen S, Chen H, Du Q, Shen J. Targeting Myeloperoxidase (MPO) Mediated Oxidative Stress and Inflammation for Reducing Brain Ischemia Injury: Potential Application of Natural Compounds. Front Physiol. 2020;11: 433. https://doi.org/10.3389/fphys.2020.00433

63. Battistuzzi G, Stampler J, Bellei M, Vlasits J, Soudi M, Furtmüller PG, et al. Influence of the covalent heme–protein bonds on the redox thermodynamics of human myeloperoxidase. Biochemistry. 2011;50(37):7987-94. https://doi.org/10.1021/bi2008432

64. Battelli MG, Polito L, Bortolotti M, Bolognesi A. Xanthine Oxidoreductase-Derived Reactive Species: Physiological and Pathological Effects. Oxid Med Cell Longev. 2016;2016:3527579. https://doi.org/10.1155/2016/3527579

65. Metz S, Thiel W. QM/MM studies of xanthine oxidase: variations of cofactor, substrate, and active-site Glu802. J Phys Chem B. 2010;114(3):1506-17. https://doi.org/10.1021/jp909999s

66. Almeida C, Monteiro C, Silvestre S. Inhibitors of 11β-Hydroxysteroid Dehydrogenase Type 1 as Potential Drugs for Type 2 Diabetes Mellitus—A Systematic Review of Clinical and In Vivo Preclinical Studies. Sci Pharm [Internet]. 2021;89(1). https://doi.org/10.3390/scipharm89010005

67. Liu H, Li L, Zhang C, Li H, Liu J, Tang C, et al. 11β-Hydroxysteroid dehydrogenase type 1 inhibitor development by Lentiviral screening based on computational modeling. Pharmacology. 2018;102(3-4):169-79. https://doi.org/10.1159/000491397

68. Bae EJ. Sirtuin 6, a possible therapeutic target for type 2 diabetes. Arch Pharmacal Res. 2017;40(12):1380-9. https://doi.org/10.1007/s12272-017-0989-8

69. Zhao S, Zhu Y-Y, Wang X-Y, Liu Y-S, Sun Y-X, Zhao Q-J, et al. Structural insight into the interactions between structurally similar inhibitors and SIRT6. Int J Mol Sci. 2020;21(7):2601.

ISSN: 2458 - 8806